

# TIME-REVERSAL IMAGING AND CLASSIFICATION FOR DISTANT TARGETS IN A SHALLOW WATER CHANNEL

*Nilanjan Dasgupta and Lawrence Carin*

Department of Electrical and Computer Engineering  
Duke University, Durham, NC 27708-0291

## ABSTRACT

Time-reversal imaging (TRI) is analogous to matched-field processing, although TRI is typically very wideband and is capable of performing target classification (in addition to localization). In this paper we apply the time-reversal technique to locate man-made cylindrical targets moving in a shallow ocean channel at long range, as well as to classify them from natural false targets like a school of fish. We present imaging and classification on simulated scattering data, for both target classes. In addition to the imaging, we explore extraction of features from the time-reversal data, with these applied to subsequent target classification. Time-reversal implementation requires a fast forward model, with that implemented here by a normal-mode model. In this paper, we present the underlying theory of TRI, feature extraction and target classification via a relevance vector machine (RVM).

## 1. INTRODUCTION

Imaging and classification of underwater objects in a shallow ocean channel has generated significant interest in the scientific community for several years. The problem is complicated due to the multipath phenomena occurring through reflections from the ocean surface and the bottom. The random fluctuations of the sea surface and the complicated bathymetry of the ocean floor make the modeling of the acoustic waves in a realistic ocean channel very difficult. The time reversal mirror [1] technique has been shown in both acoustic and ultrasonic imaging to be very effective and robust in compensating for the aberrations caused by inhomogeneities in the propagation medium, multipath and imperfections in the transceiver positions. Jackson and Dowling [2] have established the theoretical understanding of the time reversal technique applied to underwater imaging. Time-reversal imaging may be perceived as an active matched-field processing scheme where the channel itself acts as a matched filter, thus helping to identify the target scattering centers that reside within the channel. The time-reversal image is subjected to feature extraction with which we develop a target classification algorithm based on a non-linear classifier called the relevance vector machine (RVM) [3].

The paper is organized as follows: In Sec. 2 we discuss the underlying time reversal theory in an acoustic channel. In Sec. 3 we formulate the feature extraction and briefly explain the RVM classifier. Example results are presented in Sec. 4, followed by conclusions in Sec. 5.

## 2. TIME-REVERSAL THEORY

The phenomenon of time reversal has been studied by several scientists [4],[5] in both a real ocean environment and simulated acoustic medium. Previous researchers [2],[6] have already presented the physics of time reversal; hence, we briefly describe the phenomena here and concentrate on the specifics of our problem. It has been shown theoretically that if a source is completely surrounded by an arbitrary closed surface and the signal transmitted from the source is recorded at all points on the surface, then one would achieve perfect convergence at the source location by time reversing the recorded signal and sending it back into the closed cavity [2]. It is generally deemed impossible to achieve time reversal in most real-life situations, due to the physical limitation of recording at an infinite number of points on the closed surface. However, in an acoustic waveguide, one may achieve near-optimal performance by spanning the entire channel by an array of transceivers, with maximum inter-element distance of  $\lambda/2$ , where  $\lambda$  corresponds to the minimum wavelength of the transmitted signal. Assuming that our experimental scenario satisfies the requirements, the mathematical understanding of our problem is as follows.

Suppose, the signal transmitted from the source located at  $\mathbf{r}'$  is characterized by  $S(\omega)$  (frequency-domain representation). The backscattered signal received by the  $m^{\text{th}}$  receiver located at  $\mathbf{r}_m$  is given by

$$R(\omega, \mathbf{r}_m) = S(\omega) \Gamma_n(\omega) G(\omega, \mathbf{r}_{sn}, \mathbf{r}') G(\omega, \mathbf{r}_m, \mathbf{r}_{sn}) \quad (1)$$

where  $\Gamma_n$  represents the reflectivity of the  $n^{\text{th}}$  scattering center,  $G(\omega, \mathbf{r}_{sn}, \mathbf{r}')$  represents the wave propagation from the source to the scattering center and  $G(\omega, \mathbf{r}_m, \mathbf{r}')$  represents the propagation from the scattering center to the  $m^{\text{th}}$  receiver. Since launching the time-reversed signal into the waveguide is equivalent to phase conjugation in the frequency domain, the phase-conjugated signal observed after propagating from  $\mathbf{r}_m$  to point  $\mathbf{r}$  is expressed as

$$S_{TR}(\omega, \mathbf{r}) = R^*(\omega, \mathbf{r}_m) G(\omega, \mathbf{r}, \mathbf{r}_m) \quad (2)$$

Due to spatial reciprocity,  $G(\omega, \mathbf{r}_m, \mathbf{r}_{sn}) = G(\omega, \mathbf{r}_{sn}, \mathbf{r}_m)$ . Therefore, we obtain constructive interference at  $\mathbf{r} = \mathbf{r}_{sn}$ . The time-reversed signal received at  $\mathbf{r} = \mathbf{r}_{sn}$  is approximately the reflection coefficient at  $\mathbf{r}_{sn}$  convolved with the incident pulse and transmission from the source to  $\mathbf{r}_{sn}$ . At this point, we have

localized the scatterer at  $\mathbf{r}_{sm}$ , but it has the wrong time dependence due to the effects of the initial propagation through the channel. To eliminate the effects of this propagation, we again run the forward model to compute  $G(\omega, \mathbf{r}_{sm}, \mathbf{r}')$ , which finally yields the time-dependent reflection coefficient, convolved with the incident pulse, at the point of the scattering center as

$$S_{TRM}(\omega, \mathbf{r}) = R^*(\omega, \mathbf{r}_{sm})G(\omega, \mathbf{r}, \mathbf{r}_{sm})G(\omega, \mathbf{r}', \mathbf{r}) \quad (3)$$

which corresponds to the backpropagation of the received signal from  $\mathbf{r}_{sm}$  to the source via target. We perform the same process for all the receivers individually and add them together, which corresponds to phase conjugation for a single frequency  $\omega$  as follows.

$$S_{TRM}^{array}(\omega, \mathbf{r}) = \sum_{m=1}^{N_M} R^*(\omega, \mathbf{r}_{sm})G(\omega, \mathbf{r}, \mathbf{r}_{sm})G(\omega, \mathbf{r}', \mathbf{r}) \quad (4)$$

where  $N_M$  is the total number of receivers. In this way, we may achieve four-dimensional imaging of the scattering centers on a target, localizing the scattering center in 3D space, as well as the associated time dependence. Upon performing numerical time-reversal imaging, we obtain a time-domain signal at each point in 3D space. The time-dependent images, one for each receiver, add constructively at the location of the target and also identifying the time at which each scattering center has fired. We extract features from each time-reversed response at the location of target(s), with classification performed via a relevance vector machine (RVM) [3]. It is to be noted that the time-dependent TRM signal at the target location is relatively independent of target-sensor distance and numerical TRM is relatively insensitive to mismatch between numerical and actual channel.

It is observed that TRM is capable of locating the scattering centers through super-resolution [6] for man-made targets whereas we achieve very modest focusing for the school of fish. We utilize this phenomenon to extract suitable features for subsequent target classification. The phenomenon can be explained as follows.

Based on the waveguide propagation model, the acoustic pressure generated by the point source at position  $(x, y, z)$  can be represented as

$$p(x, y, z, t) = e^{-j\pi/4} \sqrt{\frac{2\pi}{z}} \sum_{m=1}^M \sin\left(\frac{m\pi}{h} y\right) \int_{-\infty}^{\infty} e^{j\omega t} e^{-\beta_m z} a_m(\omega) \sqrt{k_m} d\omega \quad (5)$$

where  $M$  is the number of modes excited,  $a_m$  is the excitation amplitude of the  $m^{\text{th}}$  mode and  $k_m = \sqrt{k^2 - \left(\frac{m\pi}{h}\right)^2}$  is the corresponding wavenumber. Via first-order saddle-point asymptotic, (5) may be rewritten as

$$p(x, y, z, t) \approx \frac{2\pi}{z} \sum_{m=1}^M \sin\left(\frac{m\pi}{h} y\right) A_m(t, z) e^{j\phi_m(t, z)} \quad (6)$$

where  $A_m(t, z) = a_m(\omega_{sm}) \frac{\omega_{sm}^2 - \omega_{cm}^2}{\omega_{cm}}$  and

$$\phi_m(t, z) = \omega_{sm} t - \frac{z}{c} \sqrt{\omega_{sm}^2 - \omega_{cm}^2}$$

$a_m$  and  $\phi_m$  are respectively the time and distance dependent amplitude and phase of the  $m^{\text{th}}$  mode and  $\omega_{cm} = \frac{m\pi c}{h}$  is the corresponding cutoff frequency.

It is evident from the above set of equations that independent of range, the time-dependent frequency settles down to the modal cutoff frequencies at late times (large  $t$ ). A fish school is a distributed set of *random* scatterers, all producing the same late-time response with random phase/amplitude. Therefore, the late-time response of a fish school tends to destructively interfere whereas man-made target has a discrete and finite set of distributed scattering centers. Also, the scattering centers in a man-made target are statistically correlated unlike in the fish school. Hence, we observe a strong late-time response for man-made targets, this subsequently resulting in significant focusing (waveform tightening) via TRM.

### 3. FEATURE EXTRACTION AND CLASSIFIER DESIGN

The sensor is assumed fixed and the target moves with respect to it. A time-reversal waveform is computed for each target-sensor orientation, as a function of range for a fixed depth. This yields a 2D aspect-range image, from which features are extracted. We extract a few simple features for every target location (each ping, corresponding to a particular target-sensor orientation). One feature used by our classifier is the ratio of the temporal (range) extent of the backscattered signal before and after TRM. We define the extent as the temporal width beyond which power of the signal is less than 30% of the peak power. The second feature utilized here incorporates the temporal extent and the energy of the signal within the temporal extent. The feature being used is the percentage energy of the whole signal within the temporal extent defined as above. A series of feature vectors is computed, one for each target-sensor orientation. At this point each feature vector is treated independently, although one might enhance the classification by combining multiple observation via a hidden Markov model (HMM) [9].

Given a feature vector for each target position/orientation (corresponding to each ping from the source to the moving target), we have a set of feature vectors for each target and natural clutter, with which we develop a single non-linear binary classifier based on the relevance vector machine (RVM) [3]. The classifier is of the form

$$f(v, w) = \sum_{n=1}^N w_n g(v, v_n) + w_0 \quad (7)$$

where  $g(v, v_n)$  is a kernel that quantifies the similarity between the feature vectors  $v$  and  $v_n$ . The weights,  $w_n$ , signify the importance of the feature vectors  $v_n$  and  $w_0$  signifies the bias. The observation corresponding to  $v$  is deemed target or otherwise depending on the sign of the function  $f(v, w)$ . The relevance vector machine optimally chooses the ‘‘relevant’’ vectors  $v_n$  (those with non-zero weights) and the corresponding weights  $w_n$ , based on the labeled training data. The expression in (7) is computed for each ping (target-sensor orientation), and a classification (target vs. clutter) is made for each, one at a time.

### 4. EXAMPLE RESULTS

The data used in this paper were generated by Naval Research Laboratory (NRL), Washington, D.C. Our objective is to use the time-reversal technique to image and classify man-made cylindrical targets moving in a shallow water channel from a school of fish. The channel depth is 150 meters and the entire channel is vertically spanned by an array of 75 equispaced

receivers as shown in Fig. 1. The isotropic source is located at a depth of 74 meters and the range of illumination of the system is approximately 20 km. The bandwidth of the sensor system is from DC to 1KHz. Fig. 2a shows the top view of the linear target tracks at four different ranges (1, 5, 10 and 15 km from the vertical receiver array located at the center) and two turning tracks are shown in Fig. 2b. The tracks followed by the school of mackerel and herring are shown in Fig. 2c and 2d, respectively. In this exercise, we have in-channel responses from two man-made targets (termed as “small” and “medium” targets). The man-made targets move through the channel at a fixed speed of 4 knots while the source pings the target at every 3 minutes. Fig. 3a shows the in-channel target-response before TRM for the entire set of pings. Fig. 3b shows the equivalent plot after TRM processing. In Fig. 4, we have taken a vertical cut on the whole image and plotted the target response at broadside as a function of target-sensor distance. Comparing Figs. 4a with 4b, it is evident that TRM results in better focusing of the target response by compensating for the multipaths.

Fig. 5 shows the comparison between the estimated target locations as derived from the time-reversed target response (by locating the position of the time-reversed peak) with respect to the ground truth. It demonstrates that the TRM is capable of locating moving targets in a shallow ocean channel. In Fig. 6, we show the target imaging by synthetic aperture sonar (SAS) processing on the time-reversal image. Specifically, the range-dependent TRM waveforms for multiple target-sensor orientations are used to constitute a synthetic aperture, with which a composite SAS image is formed. One can identify the sharply focused scattering centers. Fig. 7a and 7b shows the equivalent TRM focusing and TRM+SAS imaging for a school of mackerel. Lack of focusing on scattering centers is evident. Figs. 8a and 8b shows the response from a herring school before and after TRM (for a single ping) which demonstrates the lack of perceivable focusing through time reversal.

Given the time-reversed target responses, we perform feature extraction and design a RVM-based binary classifier. Fig. 9 plots the classifier performance based on receiver operating characteristics (ROC) for both raw and time-reversed data. We observe that at a 10% false alarm rate time reversal increases the classification performance from 10% to 80%. Note that these results used the original aspect-dependent TRM waveforms, without performing subsequent SAS processing.

## 5. CONCLUSIONS

Time-reversal imaging and classification is addressed in a shallow ocean channel. It is demonstrated that time reversal is capable of compensating for multipath in an acoustic waveguide and, for the examples considered, it increase the target classification performance significantly (even with simple features). We hope to use more physics-based features and combine multiple target responses from different orientations to enhance the classification performance even further.

## 11. REFERENCES

[1] M. Fink and C. Prada, “Acoustic time-reversal mirrors,” *Inverse problems* 17(2001).  
 [2] D. R. Jackson and D. R. Dowling, “Phase conjugation in underwater acoustics,” *J. Acoust. Soc. Am.*, 89(1), Jan. 1991.

[3] M. E. Tipping, “Sparse Bayesian learning and the relevance vector machine,” *Journal of Machine Learning Research*, No. 1, pp. 211-214, 2001. [2] M. Fink, “Time Reversed Acoustics,” *Physics Today*, March 1997.  
 [4] P. Roux and M. Fink, “Time reversal in a waveguide: Study of the temporal and spatial focusing,” *J. Acoust. Soc. Am.*, 107(5), pp. 2418-2429, May 2000.  
 [5] A. B. Baggeroer, W. A. Kuperman and P. L. Mikhalevsky, “An Overview of Matched Field Methods in Ocean Acoustics,” *IEEE Journal of Oceanic Engineering*, Vol. 18, No. 4, Oct. 1993.  
 [6] S. Kim, G. F. Edelman, W. A. Kuperman, W. S. Hodgkiss, and H. C. Song, “Spatial resolution of the time-reversal arrays in shallow water,” *J. Acoust. Soc. Am.*, 110(2), Aug. 2001.  
 [7] J. F. Lingeitch, H. C. Song and W. A. Kuperman, “Time reversed reverberation focusing in a waveguide,” *J. Acoust. Soc. Am.*, 111(6), June 2002.  
 [8] K. G. Sabra, S. R. Khosla and D. R. Dowling, “Broadband time-reversing array retrofocusing in noisy environments,” *J. Acoust. Soc. Am.*, 111(2), Feb. 2002.  
 [9] N. Dasgupta, L. Couchman and L. Carin, “Dual hidden Markov model for characterizing wavelet coefficients from multi-aspect scattering data,” *Sig. Proc.*, Vol. 81, pp. 1303-1316, 2001.

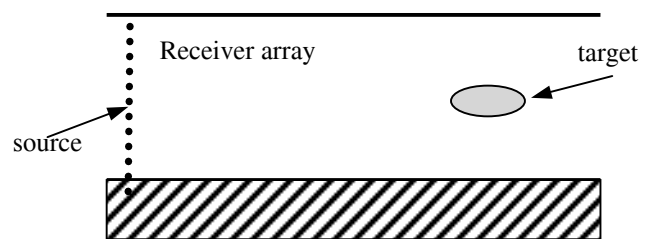


Fig. 1 Channel Model

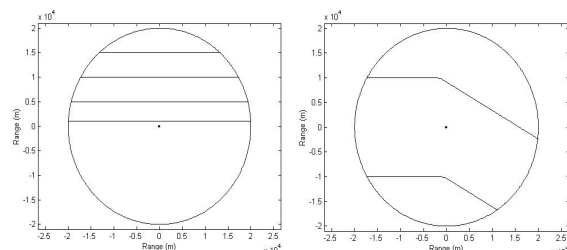


Fig. 2a

Fig. 2b

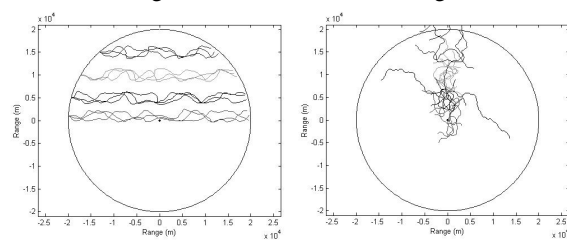


Fig. 2c

Fig. 2d

Fig. 2a Four linear tracks for man-made cylindrical targets  
 Fig. 2b Two turning tracks each man-made target.  
 Fig. 2c Four sets of tracks for mackerel school.  
 Fig. 2d Four set of tracks for herring school.

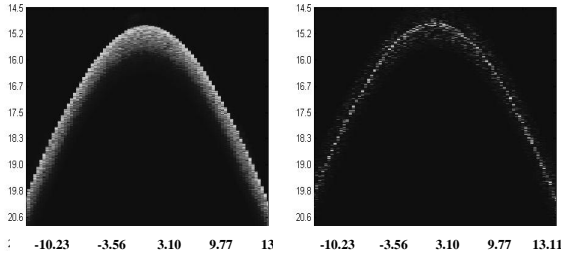
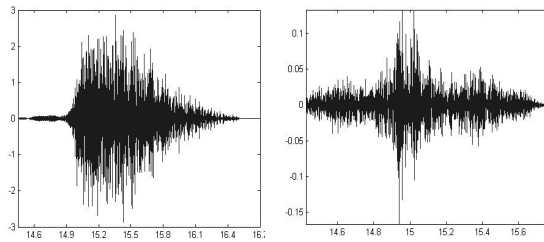


Fig. 3a

Fig. 3b

Fig. 3a In-channel response (before time-reversal) for “small” target at different positions along the linear track. The vertical axis represents the target-sensor distance in km and the horizontal axis is cross range in km.

Fig. 3b “Small” target response after time-reversal. Both axis are in km.



Cross range distances in km

Fig. 4a

Cross range distances in km

Fig. 4b

Fig. 4a In-channel response from “small” target when sensor array is at broadside and 15 km away from the target.

Fig. 4b Time-reversed response from “small” target when sensor array is at broadside and 15 km away from the target.

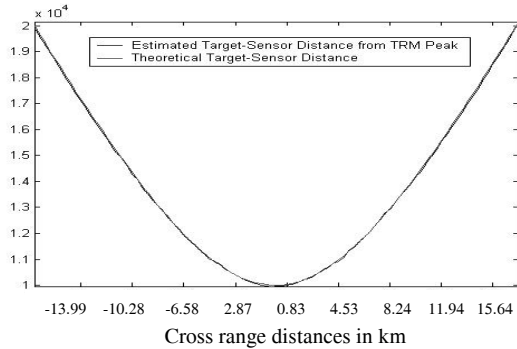


Fig. 5 Comparison between the estimated target location from the time-reversed response and the ground truth along the track.

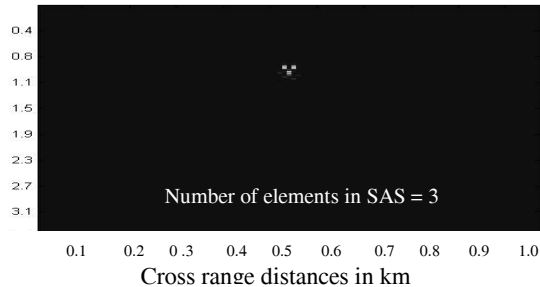
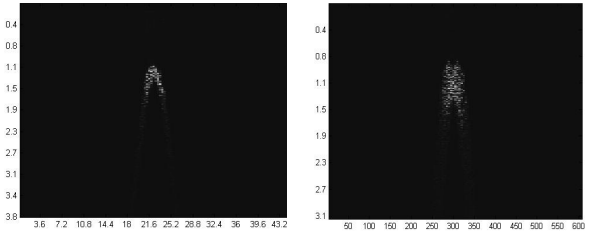


Fig. 6 “Small” target response after synthetic aperture sonar focusing on the time-reversed image. The vertical axis is target-sensor distance in km.



Cross range Distances in km

Fig. 7a

Cross range Distances in meters

Fig. 7b

Fig. 7a Time-reversed response from mackerel school as it follows a semi-linear track. The vertical axis represents target-sensor distance in km.

Fig. 7b SAS processing on time-reversed image leads to blurring unlike sharp focusing for man-made targets.

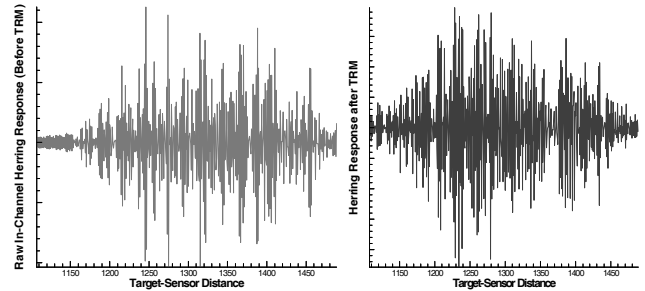


Fig. 8a

Fig. 8b

Fig. 8a In-channel herring response before TRM as a function of target-sensor distance. Horizontal axis for both plots are in km.

Fig. 8b Herring response after time reversal imaging.

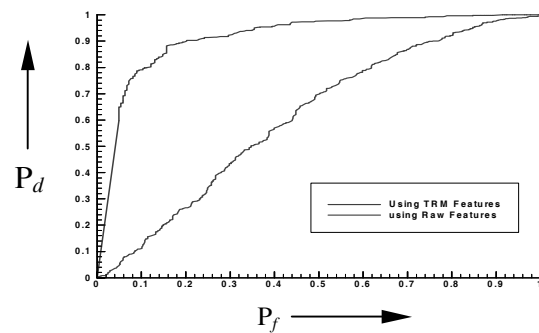


Fig. 9 Classification results based on target response before and after TRM. A single RVM classifier is used to differentiate all targets (“small” and “medium”) at all location/orientations from fish schools.